# Griffith Model Bonding in Dioxygen Complexes of Manganese Porphyrins

**Louise Karle Hanson*[1a] and Brian M. Hoffman[1b]**

*Contribution from the Division of Chemical Sciences, Department of Energy and Environment, Brookhaven National Laboratory, Upton, New York 11973, and the Department of Chemistry, Northwestern University, Evanston, Illinois 60201.* *Received January 14, 1980*

**Abstract:** The binding of $O_2$ to Mn(II) porphyrins greatly alters their optical and EPR spectra. The optical spectra of these pentacoordinate complexes are transformed from the normal to "hyper" type with a split Soret band typical of Mn(III) porphyrins. EPR spectra indicate a spin change from $S = {}^5/_2$ to $S = {}^3/_2$, and $^{17}O$ substitution reveals little unpaired spin density on the $O_2$. Contradictory interpretations of the electronic and geometric structures of these complexes have recently been advanced: analysis of the EPR data supports a "$d^3$" $Mn^{IV}O_2^{2-}$ with $O_2$ bound in the Griffith mode (edge-on, parallel to the porphyrin plane) whereas ab initio calculations favor a "$d^2\pi^*$" $Mn^{III}O_2^-$ with $O_2$ bound in the Pauling mode (end-on, bent). We report here charge iterative extended Hückel calculations on both Griffith and Pauling models of oxymanganese porphine, in which the O–O, Mn–O, and out-of-plane Mn distances and the O–O orientation above the porphinato plane were varied. For all the calculations, the porphine ring as well as the metal transfers considerable charge density onto the $O_2$, suggesting that a formal charge description of these complexes solely in terms of the $O_2Mn$ core is an oversimplification. The resultant wave functions were used to calculate $^{55}Mn$ and $^{17}O$ hyperfine splittings. Griffith models with three unpaired electrons occupying orbitals of predominantly d character give excellent agreement with the observed $^{55}Mn$ and $^{17}O$ values. Models with an unpaired electron in a predominantly dioxygen orbital are ruled out. The optical hyperspectra can be ascribed to porphine $\pi \rightarrow d_\pi, O_2\pi^*$ charge-transfer transitions that mix with the porphine $\pi \rightarrow \pi^*$ Soret transitions. Only the Griffith models place these charge-transfer transitions at favorable energies. Thus all the experimental results can be explained in terms of a $d^3$ configuration and Griffith binding of the dioxygen but *not* Pauling binding. The Griffith geometry with molecular orbital energies most consistent with the optical spectra and which best fits the observed $^{55}Mn$ and $^{17}O$ hyperfine splittings has the Mn $\sim$0.5 Å out-of-plane toward the $O_2$, a long, "peroxo", O–O bond, and the O–O staggered with respect to the pyrrole nitrogens.

Manganese(II) porphyrins ($Mn^{II}P$) in organic solvents reversibly bind molecular oxygen at low temperatures,[2-5] and the resulting dioxygen adducts differ markedly from those of cobalt and iron porphyrins.[6-8] The molecular oxygen either replaces the axial ligand, L, of $L-Mn^{II}P$ complexes or adds to ligand-free manganese(II) porphyrins[9] to form the pentacoordinate oxymanganese complex $O_2MnP$. This is in contrast to the hexacoordinated oxy complexes formed by iron and cobalt porphyrins in both solution and protein environments. Dioxygen binding by manganese(II) porphyrins transforms[2,4] the optical spectrum from a normal metalloporphyrin type to a "hyper" type,[10] typified by multiple or "split" Soret bands whereas oxyiron and oxycobalt porphyrins exhibit normal optical spectra. Electron paramagnetic resonance (EPR) spectra of the manganese porphyrins[2,4,5] indicate a change from high spin, $S = {}^5/_2$, to intermediate spin, $S = {}^3/_2$, upon binding of $O_2$, and $^{17}O$ substitution shows that little unpaired spin density resides on the $O_2$. This is again in contrast to oxyiron and oxycobalt complexes which are low spin and, in the case of oxycobalt, have significant unpaired spin density residing[8] on the $O_2$. These differences, ongoing studies of manganoglobin,[11] and manganese-substituted hemoglobin, and the possible use of manganese porphyrins as oxygenation catalysts[12] combine to make a detailed understanding of the $O_2MnP$ adducts of chemical and biochemical interest.

A ligand field analysis of the EPR results led to the conclusion that the $O_2$ molecule binds to an out-of-plane manganese in the Griffith (edge-on) geometry (Figure 1) in one of only two possible odd-electron configurations[5] ($d_{x^2-y^2}$, $d_{xz}$, $d_{yz}$, and $d_{x^2-y^2}$, $d_{xz}$, $d_{z^2}$),[13] both of which are interpretable in a $Mn^{IV}O_2^{2-}$ formalism. Nonetheless, ab initio calculations[14] predicted that the most stable odd-electron configuration is $Mn^{III}O_2^-$, with an unpaired electron in a dioxygen $\pi^*$ orbital and the $O_2$ bound in the Pauling (end-on, bent) geometry (Figure 1) as in oxyiron and oxycobalt complexes. The optical spectra are consistent with such an interpretation since Mn(III) porphyrins characteristically exhibit hyperspectra.[15]

In order to obtain a better understanding of the EPR results and to resolve the apparent contradictions concerning the electronic and geometric structures of oxymanganese porphyrins, we have performed charge iterative extended Hückel (IEH) calculations on oxymanganese porphine complexes with $O_2$ bound in both the Griffith and Pauling geometries,[16] calculated $^{55}Mn$ and $^{17}O$ hyperfine splittings from the resultant wave functions, and analyzed the optical spectra. The extended Hückel method was chosen because of its success in describing the metal–ligand–porphine electronic interactions of metalloporphyrins.[10,17-19] In the present calculations, the O–O, Mn–O, and Mn out-of-plane distances and the O–O orientation relative to the porphinato nitrogens were varied to accommodate superoxide and peroxide dioxygen bond

(1) (a) Brookhaven National Laboratory. (b) Northwestern University.
(2) Weschler, C. J.; Hoffman, B. M.; Basolo, F. *J. Am. Chem. Soc.* **1975**, *97*, 5278–80.
(3) Gonzalez, B.; Kouba, J.; Yee, S.; Reed, C. A.; Kirner, J. F.; Scheidt, W. R. *J. Am. Chem. Soc.* **1975**, *97*, 3247–9.
(4) Hoffman, B. M.; Weschler, C. J.; Basolo, F. *J. Am. Chem. Soc.* **1976**, *98*, 5473–82.
(5) Hoffman, B. M.; Szymanski, T.; Brown, T. G.; Basolo, F. *J. Am. Chem. Soc.* **1978**, *100*, 7253–9.
(6) (a) Jones, R. D.; Summerville, D. A.; Basolo, F. *Chem. Rev.* **1979**, *79*, 139–79. (b) James, B. R. In "The Porphyrins"; Dolphin, D., Ed.; Academic Press: New York, 1978; Vol. V, pp 205–302.
(7) (a) Basolo, F.; Hoffman, B. M.; Ibers, J. A. *Acc. Chem. Res.* **1975**, *8*, 384–92. (b) Vaska, L. *Ibid.* **1976**, *9*, 175–83.
(8) (a) Hoffman, B. M.; Diemente, D. L.; Basolo, F. *J. Am. Chem. Soc.* **1970**, *92*, 61–5. (b) Vansant, E. F.; Lunsford, J. H. *Adv. Chem. Ser.* **1973**, *No. 121*, 441–7.
(9) (a) Jones, R. D.; Summerville, D. A.; Basolo, F. *J. Am. Chem. Soc.* **1978**, *100*, 4416–24. (b) Basolo, F.; Jones, R. D.; Summerville, D. A. *Acta Chem. Scand., Ser. A* **1978**, *A32*, 771–80.
(10) Gouterman, M. In "The Porphyrins"; Dolphin, D., Ed.; Academic Press: New York, 1978; Vol. III, pp 1–166.
(11) Gibson, Q. H.; Hoffman, B. M. *J. Biol. Chem.* **1979**, *254*, 4691–7 and references cited therein.
(12) Jahnke, H.; Schönborn, M.; Zimmerman, G. *Top. Curr. Chem.* **1976**, *61*, 133–81.
(13) The nomenclature corresponds to $x$ and $y$ axes defined by the bridging methine carbons of the porphine ring.
(14) (a) Dedieu, A.; Rohmer, M. M. *J. Am. Chem. Soc.* **1977**, *99*, 8050–1. (b) Dedieu, A.; Rohmer, M. M.; Veillard, H.; Veillard, A. *Nouv. J. Chim.* **1979**, *3*, 653–67.
(15) Boucher, L. J. *Ann. N.Y. Acad. Sci.* **1973**, *206*, 409–19.
(16) Accounts of this work were presented at the 23rd Annual Meeting of the Biophysical Society, Feb 1979. Hanson, L. K.; Hoffman, B. M. *Biophys. J.* **1979**, *25*, 185a; and the March 1979 Sanibel Symposium on Quantum Biology and Quantum Pharmacology.[19]
(17) Hanson, L. K.; Eaton, W. A.; Sligar, S. G.; Gunsalus, I. C.; Gouterman, M.; Connell, C. R. *J. Am. Chem. Soc.* **1976**, *98*, 2672–4.
(18) Eaton, W. A.; Hanson, L. K.; Stephens, P. J.; Sutherland, J. C.; Dunn, J. B. R. *J. Am. Chem. Soc.* **1978**, *100*, 4991–5003.
(19) Hanson, L. K. *Int. J. Quantum Chem., Quantum Biol. Symp.* **1979**, *6*, 73–87.

0002-7863/80/1502-4602$01.00/0 

Table I. Model Geometries and Charge Densities for Selected Manganese Porphine Calculations

| ligand | MnP models: Mn–Ct,[a] Å | MnP models: Mn–O, Å | MnP models: O–O, Å | pyrrole N···O,[b] Å | charge densities: axial ligand[c] | charge densities: Mn | charge densities: porphine ring[c] |
|---|---|---|---|---|---|---|---|
| $O_2$ Griffith | | | | | | | |
| N eclipsed | 0.51 | 1.85 | 1.49 | 2.70 | −0.535 | 0.166 | 0.369 |
| | 0.19 | 2.09 | 1.49 | 2.64 | −0.519 | 0.169 | 0.350 |
| | 0.19 | 2.02 | 1.49 | 2.64 | −0.454 | 0.162 | 0.292 |
| | 0.25 | 1.63 | 1.25 | 2.32[d] | −0.451 | 0.184 | 0.267 |
| $C_m$ eclipsed[e] | 0.51 | 1.85 | 1.49 | 2.85 | −0.562 | 0.159 | 0.403 |
| | 0.51 | 1.85 | 1.26 | 2.88 | −0.501 | 0.157 | 0.343 |
| | 0.51 | 1.63 | 1.26 | 2.70 | −0.465 | 0.192 | 0.273 |
| | 0.19 | 1.95 | 1.49 | 2.67 | −0.530 | 0.180 | 0.350 |
| | 0.19 | 1.95 | 1.26 | 2.71 | −0.453 | 0.172 | 0.281 |
| $a_{2u}(\pi) \rightarrow e_{gy}(\pi^*)$[f] | 0.51 | 1.85 | 1.49 | | −0.527 | 0.199 | 0.326 |
| $a_{2u}(\pi) \rightarrow d_{yz} - O_2\pi_{gz}$[f] | 0.51 | 1.85 | 1.49 | | −0.633 | 0.142 | 0.490 |
| $O_2$ Pauling | | Mn–O | | | | | |
| | 0.51 | 1.85 | 1.49 | 3.1 | −0.520 | 0.163 | 0.357 |
| | 0.51 | 1.85 | 1.25 | 3.1 | −0.404 | 0.148 | 0.256 |
| | 0.19 | 1.85 | 1.49 | 2.9 | −0.496 | 0.167 | 0.328 |
| | 0.19 | 1.85 | 1.25 | 2.9 | −0.383 | 0.151 | 0.232 |
| none ($S = {}^5/_2$) | | | | | | | |
| | 0.51 | | | | | 0.084 | −0.084 |
| | 0.19 | | | | | 0.102 | −0.102 |
| pyridine ($S = {}^5/_2$) | | Mn–N | | | | | |
| | 0.51 | 2.19 | | | 0.259 | 0.065 | −0.325 |

[a] Displacement of the Mn from the porphine plane. Ct = center of the ring. [b] The van der Waals contact distance for N···O is 2.9 Å. N···O = 2.64 Å in the eclipsed peroxotitanium(IV) octaethylporphine, $O_2Ti^{IV}OEP$, crystal structure.[28] [c] Sum of the charge densities of all the atoms of the axial ligand or porphine ring, respectively. [d] Coordinates used by Dedieu and Rohmer in their ab initio calculations[14a] on $O_2$-MnP. Their porphine ring radius, pyrrole N···Ct, was 1.972 Å. [e] $C_m$ = bridging methine carbons of the porphine ring. [f] Excited states.

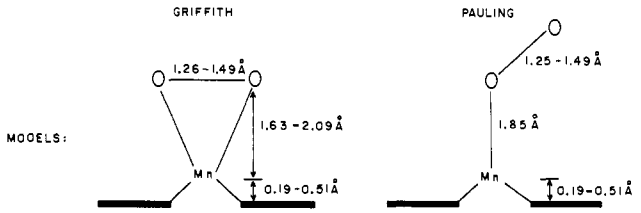


**Figure 1.** Oxymanganese porphine models used in the calculations: left, the Griffith geometries with the dioxygen bound edge-on, parallel to the porphine ring, and, right, the Pauling geometries with the dioxygen bound end-on and bent. Shown are the ranges in the Mn out-of-plane displacement, and Mn–dioxygen and O–O distances which were considered.

distances, known manganese(II) porphyrin crystal structures, and nonbonded constraints between the axial ligand and the porphine ring. The calculations succeed in providing a geometry-dependent molecular orbital description of oxymanganese porphyrins in terms of the Griffith model which is consistent with both the optical and magnetic data.

## Methods

The program used for these calculations was written by Davidson[20] and was kindly provided by M. Gouterman, University of Washington. The χ, H, N, C, O, and Mn parameters were those of Zerner et al.[21] A major asset of the charge iterative extended Hückel method is its flexibility: there are no constraints on atom type, atomic orbital type (s, p, and d atomic orbitals were included), or model geometries, and the molecular orbital occupancies can be specified. EPR spectral simulations were performed with Program SIM 14, available through the Quantum Chemistry Program Exchange, Bloomington, Ind., as Program No. 265.

## Model Geometries

Oxymanganese porphines with $O_2$ bound in both the Pauling (end-on) and Griffith (edge-on) geometries were calculated with the manganese displaced either 0.19 or 0.51 Å from the pyrrole nitrogen plane (Figure 1). These distances correspond to those found in crystal structures of *m*-(tetraphenylporphinato)manganese(II) (MnTPP)[3] and *m*-(tetraphenylporphinato)manganese(II) 1-methylimidazole ((1-MeIm)-$Mn^{II}$TPP),[3,22] respectively. The porphinato core geometries for each structure were idealized to $D_{4h}$ symmetry and used with the appropriately displaced manganese. The more coplanar the manganese, the more expanded the porphinato core, 2.065 Å for the Mn 0.51-Å displacement and 2.082 Å for the Mn 0.19-Å displacement.

In both the Pauling and Griffith calculations, the O–O distance was varied between values for superoxide ($O_2^-$, 1.25 or 1.26 Å) and peroxide ($O_2^{2-}$, 1.49 Å). In the Pauling calculations the $O_2$ is staggered with respect to the nitrogens; and Mn–O = 1.85 Å, based on the Fe–O distances in the oxyiron "picket fence" porphyrin structures[23] and taking into account the larger ionic radius of Mn(II). In the Griffith calculations, Mn–$O_2$ midpoint distances were varied between 1.63 and 2.09 Å depending upon the O–O distance, the Mn out-of-plane displacement, and the O–O orientation above the porphinato plane (staggered or eclipsed with respect to the pyrrole nitrogens). The critical factor governing the $O_2$ distance from the Mn is steric constraint with the porphine: the pyrrole N···O nonbonded interactions. The Griffith model geometries and the resulting pyrrole N···O distances are given in Table I. The van der Waals contact distance for N···O is 2.9 Å.

For the (pyridine)manganese(II) porphine calculations, the Mn–pyridine N distance was set at 2.19 Å, the Mn–axial N distance determined in the crystal structure analysis of (1-MeIm)$Mn^{II}$TPP.

The porphine defines the *xy* plane. *x* and *y* are along the bridging (methine) carbons for calculations where the $O_2$ is staggered with respect to the pyrrole nitrogens. For calculations with an eclipsed $O_2$, *x* and *y* are along the pyrrole nitrogens. The axial ligand defines the *yz* plane.

## Results and Discussion

**Orbitals and Orbital Energies**: Representative orbital energy diagrams calculated for high-spin, $S = {}^5/_2$, (pyridine)manganese(II) porphine, (py)$Mn^{II}$P, and intermediate-spin, $S = {}^3/_2$, oxyMn porphines, $O_2$MnP, with $O_2$ bound in the Griffith and

(20) Schaffer, A. M.; Gouterman, M.; Davidson, E. R. *Theor. Chim. Acta* **1973**, *30*, 9–30.

(21) (a) Zerner, M.; Gouterman, M. *Theor. Chim. Acta* **1966**, *4*, 44–63. (b) Zerner, M.; Gouterman, M.; Kobayashi, H. *Ibid.* **1966**, *6*, 363–400.

(22) Kirner, J. F.; Reed, C. A.; Scheidt, W. R. *J. Am. Chem. Soc.* **1977**, *99*, 2557–63.

(23) (a) Jameson, G. B.; Rodley, G. A.; Robinson, W. T.; Gagne, R. R.; Reed, C. A.; Collman, J. P. *Inorg. Chem.* **1978**, *17*, 850–7. (b) Jameson, G. B.; Molinaro, F. S.; Ibers, J. A.; Collman, J. P.; Brauman, J. I.; Rose, E.; Suslick, K. S. *J. Am. Chem. Soc.* **1978**, *100*, 6769–70.

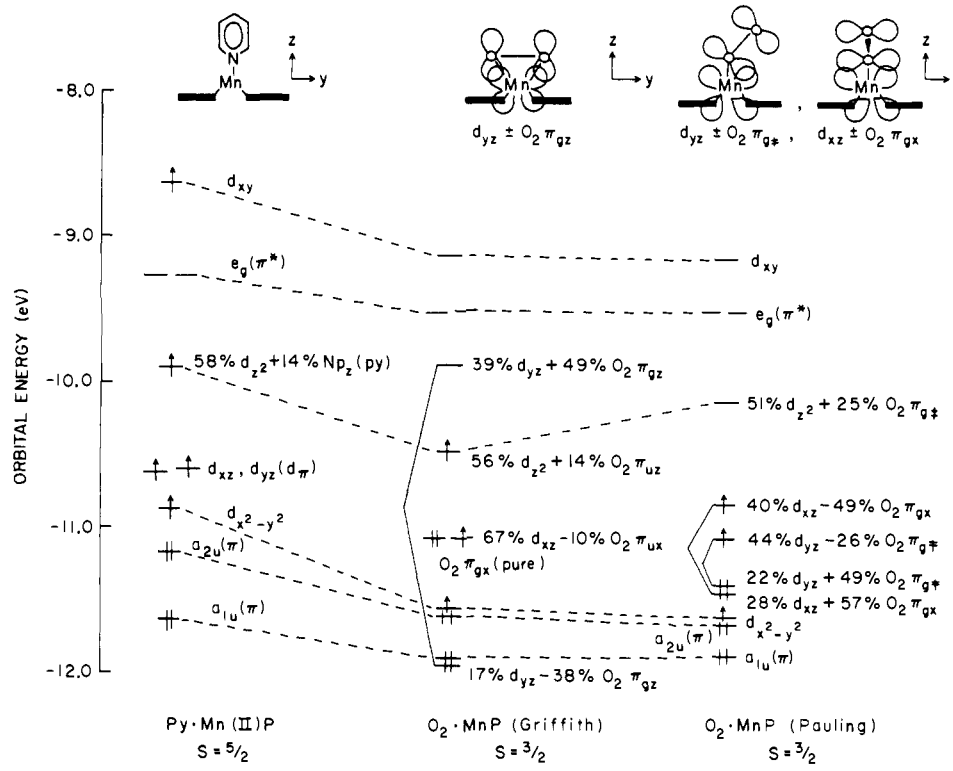


**Figure 2.** Comparison of the calculated orbital energies for (pyridine)manganese porphine, left, and oxyMn porphine with the $O_2$ bound in Griffith (center) and Pauling (right) geometries. The structural parameters for the oxy calculations are as follows: Mn out-of-plane displacement = 0.51 Å, O–O = 1.49 Å, Mn–O = 1.85 Å (Pauling mode), Mn–$O_2$ midpoint = 1.85 Å (Griffith mode), and the dioxygen is staggered with regard to the pyrrole nitrogens. For the Pauling calculation, $O_2\pi_{g\ddagger}$ denotes the dioxygen $\pi_g$ orbital which is in the *yz* plane and is a linear combination of oxygen $p_y$ and $p_z$ atomic orbitals.

Pauling geometries are shown in Figure 2. The (py)$Mn^{II}P$ results are typical for a high-spin five-coordinate metalloporphyrin and closely resemble the molecular orbitals obtained for $S = 2$, (pyridine)$^{10}$- or (imidazole)iron(II)[18,19] porphine complexes. The only metal–axial ligand interaction is the $\sigma$ bonding between the metal $d_{z^2}$ and the axial nitrogen $p_z$ orbitals.

The five-coordinate oxyMn complexes have much more extensive metal–axial ligand interactions. The Mn $d_\pi$ ($d_{xz}$, $d_{yz}$) and dioxygen $\pi_g$ orbitals mix to form hybrid orbitals, the degree of mixing depending upon the $O_2$-binding geometry. In the Griffith case, the $d_\pi$ orbital in the symmetry plane defined by the dioxygen, $d_{yz}$, and the $O_2\pi_{gz}$ orbital form a bonding and an antibonding pair, $d_{yz} \pm O_2\pi_{gz}$. The $O_2\pi_{gx}$ and $d_{xz}$ orbitals remain unmixed. In the Pauling case, both $d_\pi$ orbitals mix with both $O_2\pi_g$ orbitals, creating four hybrid orbitals, $d_{xz} \pm O_2\pi_{gx}$ and $d_{yz} \pm O_2\pi_{g\ddagger}$ ($\ddagger$ denotes a mixture of $Op_y$ and $Op_z$). The $d_{z^2}$ orbital has minimal overlap with the dioxygen orbitals when $O_2$ binds in the Griffith geometry, whereas there is considerable $\sigma$ bonding to the axial $Op_z$ orbital in the Pauling geometry. Hence the $d_{z^2}$ lies at lower energy in the Griffith geometry.

The splitting between the Griffith $d_{yz} \pm O_2\pi_{gz}$ hybrid orbitals is much larger than the splitting between the four Pauling $d_\pi$,$O_2\pi_g$ hybrid orbitals. This places an antibonding $d_\pi$,$O_2\pi_g$ orbital at a significantly higher energy in the Griffith model, indeed, above the $d_{z^2}$ orbital. The actual calculated energy of this $d_{yz} + O_2\pi_{gz}$ orbital is extremely sensitive to factors which affect the $d_{yz}$,$O_2\pi_{gz}$ overlap such as the vertical Mn–$O_2$ distance and the O–O bond length. Figure 3 shows that shortening the vertical Mn–O distance has the greatest effect on strengthening the $d_{yz}$,$O_2\pi_{gz}$ overlap, increasing the hybrid orbital splitting, and raising the $d_{yz} + O_2\pi_{gz}$ orbital energy. The effect is exaggerated when the vertical Mn–$O_2$ distance is short (1.63 Å). On the other hand, changes in Mn–O and O–O distances exert little influence on $d_\pi$,$O_2\pi_g$ hybrid orbital energies of the Pauling models.

An additional feature of interest in Figure 3 is the geometry dependence of the $O_2\pi_{gx}$ orbital energy in the Griffith calculations (the Pauling models do not possess any pure $O_2\pi_g$ orbitals). This orbital is most sensitive to the O–O distance, decreasing in energy

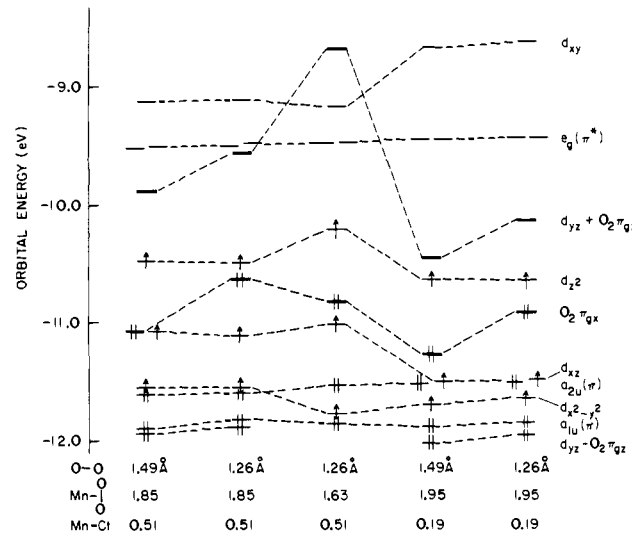


**Figure 3.** Calculated orbital energies of Griffith models of oxyMn porphine with various Mn–$O_2$, O–O, and Mn–Ct (Ct = center of the porphine ring) distances. The dioxygen is staggered with respect to the pyrrole nitrogens.

as the dioxygen bond is lengthened, which suggests that the propensity of the $O_2$ to accept electrons increases with a "peroxo" bond. Even with a "superoxo" length, however, the $O_2\pi_{gx}$ orbital remains below the $d_{z^2}$ orbital.

Figure 4 compares in detail calculations for a Griffith geometry with the pyrrole nitrogens both staggered and eclipsed by the O–O. The two calculations are nearly identical except that, in the eclipsed form, there is a slight mixing between the $d_{xy}$ and the $O_2\pi_{gx}$ orbitals. The predominantly $d_{xy}$ orbital lies below the predominantly $O_2\pi_{gx}$ orbital. Thus all the Griffith models exhibit the following orbital patterns: $d_{yz} - O_2\pi_{gz} < d_{x^2-y^2} < d_{xz}$,$O_2\pi_{gx} < d_{z^2} < d_{yz} + O_2\pi_{gz} < d_{xy}$ (*x* and *y* along porphine methine carbons), whereas the orbital sequence $d_{x^2-y^2} < d_{xz} + O_2\pi_{gx} < d_{yz} + O_2\pi_{g\ddagger}$

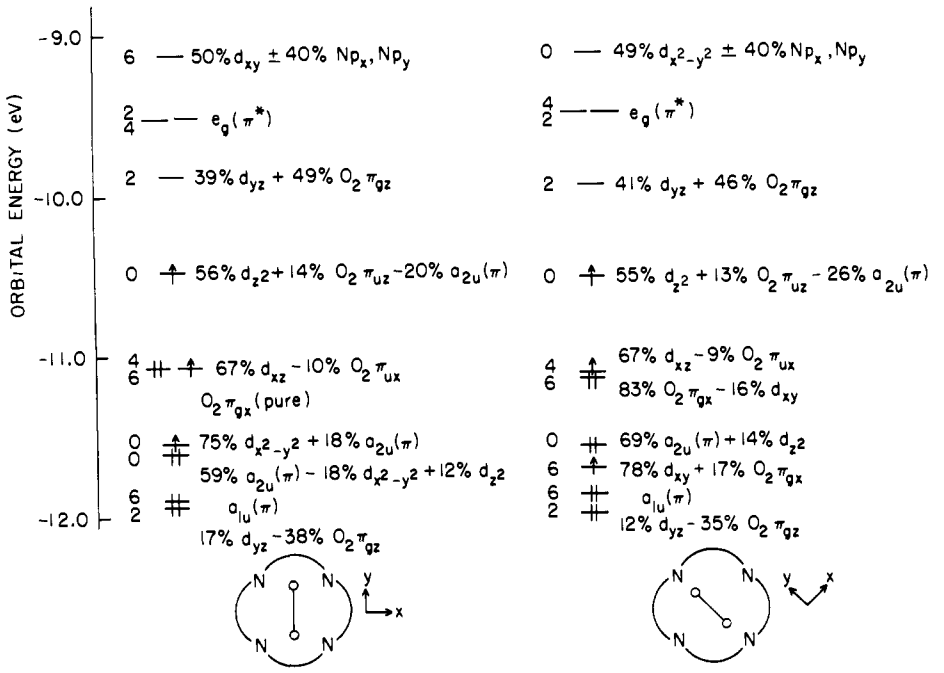


**Figure 4.** Detailed comparison of the molecular orbital coefficients and energies of staggered (left) and eclipsed (right) Griffith models of an oxyMn porphine. Other than the orientation of the dioxygen relative to the porphinato nitrogens, the structural parameters for both computations were the same: Mn–Ct = 0.51 Å, Mn–$O_2$ midpoint = 1.85 Å, and O–O = 1.49 Å. The numbers to the left of the orbitals are symmetry labels: 0, totally symmetric; 2, antisymmetric with respect to the *xy* plane; 4, antisymmetric with respect to the *yz* plane; and 6, antisymmetric with respect to the *xz* and *yz* planes.

$< d_{yz} - O_2\pi_{g\ddagger} < d_{xz} - O_2\pi_{gx} < d_{z^2} < d_{xy}$ is calculated for the Pauling models.

**EPR Analysis.** The very different EPR spectra of oxymanganese[2,4,5] and (pyridine)manganese[2,4] porphyrins can be rationalized in terms of the IEH results. The oxyMn complexes are $S = {}^3/_2$ with negligible spin density on the dioxygen ($^{17}O$ hyperfine coupling constants are ~2.5 G compared to the ~20–30 G expected[5] for a single, unpaired electron on the $O_2$) and have large zero-field splittings ($|D| = 2$–$3.2$ cm$^{-1}$), large rhombic distortions ($D/E > 0.3$), and highly anisotropic $^{55}Mn$ hyperfine splittings (53 and 88 G). In contrast, (py)Mn$^{II}$TPP is $S = {}^5/_2$ and axially symmetric ($E \approx 0$), with much smaller zero-field splittings ($|D| = 0.55$ cm$^{-1}$) and isotropic $^{55}Mn$ hyperfine splittings of 74 G. These data will be discussed from two points of view: first, by inspection of the molecular orbitals, and second, through calculation of $^{55}Mn$ and $^{17}O$ hyperfine parameters using the IEH wave functions.

The $O_2Mn$ center has a total of seven electrons, three unpaired, within the Mn d and $O_2\pi_g$ orbitals. The assignment of the occupancy of these orbitals, shown in Figure 2 was based upon two assumptions: (1) that orbital occupancy is confined to the five lowest energy d,$O_2\pi_g$ orbitals (any other electron distribution would be energetically unfeasible), and (2) that $O^{17}$ hyperfine interactions are small only when the three unpaired electrons occupy orbitals of predominantly d character. The validity of the second assumption is discussed below. In the Griffith models, these criteria lead to double occupancy of the $d_{yz} - O_2\pi_{gz}$ and $O_2\pi_{gx}$ orbitals and single occupancy of the $d_{x^2-y^2}$, $d_{xz}$, and $d_{z^2}$ orbitals. None of the latter have appreciable $O_2$ contributions (<14%). However, it is not possible to place three unpaired electrons into the low-energy orbitals of the Pauling models without singly occupying $d_\pi$,$O_2\pi_g$ hybrid orbitals which contain up to 50% $O_2$ contributions. Thus, inspection of the molecular orbitals clearly suggests that the $^{17}O$ data, which show very small oxygen hyperfine interactions, favor the Griffith geometry.

Examination of Figure 2 also suggests why pyridine complexes exhibit axially symmetric EPR spectra whereas oxy complexes have extremely rhombic spectra. The binding of pyridine does not affect the orbital degeneracy of $d_{xz}$ and $d_{yz}$. The binding of $O_2$, however, especially in the Griffith geometry, destroys the equivalence of $d_{xz}$ and $d_{yz}$, and their energies, degrees of mixing with dioxygen orbitals, and electron occupancies diverge. Small variations in the degree of rhombicity are found for oxyMn porphyrins.[5] These may be due to small geometry differences between the various porphyrin skeletons which might subtly affect the dioxygen bonding and the $O_2$,$d_{yz}$ overlap.

The large zero-field splittings ($D$ values) of oxyMn porphyrins can be similarly rationalized. These splittings are ascribable to the mixing of low-lying excited states with the ground state by a spin–orbit coupling mechanism.[24] The nonequivalent d orbital populations that are calculated for the singly occupied MO's enhance these mixing terms. Furthermore, the presence of low-lying dioxygen orbitals provides additional low-lying excited states which may also contribute.

Comparison of observed $^{55}Mn$ and $^{17}O$ hyperfine (hf) parameters with values calculated by a ligand field approach can also be used to assess various Mn–$O_2$ geometries and odd-electron configurations. A previous ligand field analysis of the EPR data favored[2,4,5] Griffith binding of dioxygen to manganese porphyrins and suggested[5] two possible d orbital configurations to account for the anisotropic $^{55}Mn$ hyperfine splittings (hfs). One of these, $d_{x^2-y^2}$, $d_{xz}$, and $d_{z^2}$, corresponds with the present IEH results. Although this configuration was considered less favorable in terms of the criterion used to test goodness of fit, i.e., agreement of a calculated $^{55}Mn$ electron nuclear coupling parameter $P^{Mn}$ with the Mn(III) and Mn(IV) free-electron values, the original analysis used 100% d orbital occupancies. If $P^{Mn}$ is recalculated with the partial occupancies of the IEH orbitals, an excellent agreement is obtained (vide infra).

$P^{Mn}$ and $^{17}O$ hfs are calculated in the Appendix for several odd-electron configurations of the Pauling as well as staggered and eclipsed Griffith geometries by substitution of IEH orbital occupancies into a ligand field formalism. The calculated splittings confirm the orbital assignments of Figure 2. Singly populating the top three occupied orbitals of both geometries [$(d_{z^2})^1(d_{xz})^1$-$(O_2\pi_{gx})^1$ for the Griffith model and three $d_\pi$,$O_2\pi_g$ hybrid orbitals for the Pauling model] yields unreasonable $^{55}Mn$ and $^{17}O$ hf parameters. The $^{17}O$ values are especially bad, as shown by the

(24) Wertz, J. E.; Bolton, J. R. "Electron Spin Resonance, Elementary Theory and Practical Applications"; McGraw-Hill: New York, 1972.

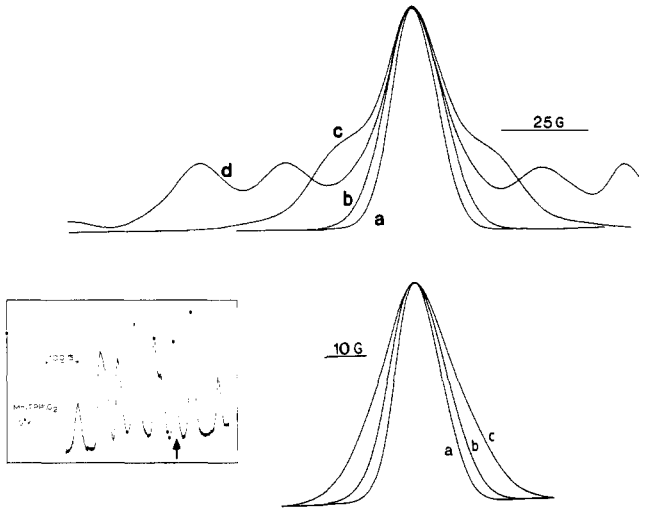


**Figure 5.** Computer simulations of a single $^{55}Mn$ hyperfine (hf) line from the EPR spectrum of the lower Kramers doublet of $O_2MnTPP$. The $g = 5.4$ region of the $^{16}O_2MnTPP$ spectrum is reproduced in the inset (lower left), and the simulated line is indicated by the arrow. Equivalent results are obtained from the highest field line, which belongs to the upper Kramers doublet. Top: (a) reproduces the line for $^{16}O_2MnTPP$, by using a Gaussian line shape with a line width of 16 G; (b) reproduces the line for $O_2MnTPP$ with 51.6% $^{17}O_2$ (The calculation assumes equivalent oxygens bound in the Griffith mode and an isotropic $^{17}O$ hfs of $a = 2.8 \times 10^{-4}$ cm$^{-1}$.); (c) $^{55}Mn$ hf line predicted for $^{17}O_2MnP$, Pauling mode, with three $d_\pi,O_2\pi_g$ hybrid orbitals singly occupied (The field is along the $x$ direction, for which both oxygen atoms are computed to have principal values greater than $9.3 \times 10^{-4}$ cm$^{-1}$ (10 G), as shown in the Appendix. A similar pattern would occur with the field along $y$ or $z$.); (d) $^{55}Mn$ hf line predicted for $^{17}O_2MnP$, Griffith mode, with a $d^2\pi^*$ one-electron configuration (The field is along the $^{17}O$ hfs tensor $y$ axis (see Appendix).). Bottom: (a) and (b) are the same as (a) and (b) above; (c) $^{55}Mn$ hf line predicted for $^{17}O_2MnP$ with an eclipsed Griffith geometry and a $d^3$ one-electron configuration (The field is along the $^{17}O$ tensor direction calculated to have a coupling of $5.6 \times 10^{-4}$ cm$^{-1}$ (see Appendix).). The staggered Griffith model with a $d^3$ one-electron configuration corresponds well to curve b.

calculated line widths in Figure 5. However, the Pauling and staggered and eclipsed Griffith models with the orbital occupancies shown in Figures 2 and 4 [$(d_{x^2-y^2}$ or $d_{xy})^1(d_{xz})^1(d_{z^2})^1$, Griffith geometry, and $(d_{x^2-y^2})^1(d_{yz} - O_2\pi_{g\pm})^1(d_{xz} - O_2\pi_{g\mp})^1$, Pauling geometry] are all consistent with the observed $^{55}Mn$ hf couplings. The calculated $^{17}O$ hfs are somewhat more discriminating. The values for the staggered Griffith structure are small, in excellent agreement with the experiment, whereas the greater spin density on the dioxygen in the eclipsed Griffith structure results in significantly larger $^{17}O$ hf couplings and simulated line widths (Figure 5). The Pauling configuration of Figure 2 places substantial spin density on the dioxygen. The hfs calculations show that it is possible for this model to give rise to the small observed $^{17}O$ broadenings, but only if the relative orientations of the fine-structure and hyperfine-interaction tensors fortuitously correspond. On this basis, we consider the Pauling geometry to be less favorable. In conclusion, although the analysis does not rigorously exclude the Pauling geometry, the staggered Griffith geometry with a $d^3$ odd-electron configuration yields the best agreement with all the EPR data.

**Optical Analysis.** The Griffith model calculations, but not those for the Pauling models, are consistent with the optical data. Oxymanganese porphyrins exhibit hyperspectra; that is, their Soret bands are split into two components, blue- and red-shifted with respect to the normal Soret position. Theoretical and experimental studies of hyperspectra in a variety of metalloporphyrins have led to the hypothesis[10,17,19] that metalloporphyrin–ligand complexes with a charge-transfer transition which has the same symmetry and energy as the porphyrin Soret $\pi$–$\pi^*$ transitions will manifest hyperspectra. The charge-transfer transition and the Soret $a_{1u},a_{2u}(\pi) \rightarrow e_g(\pi^*)$ transitions mix, splitting into high- and low-energy components which share the Soret intensity. In the oxymanganese systems, porphine $a_{1u},a_{2u}(\pi) \rightarrow d_\pi + O_2\pi_g$ charge-transfer transitions fit the symmetry criterion. Only the Griffith models have their acceptor $d_{yz} + O_2\pi_{gz}$ orbitals lying sufficiently near the porphine $e_g(\pi^*)$ orbitals (Figures 2 and 3) to allow mixing between the charge-transfer and porphine $\pi \rightarrow \pi^*$ transitions.

The Pauling model $d_\pi,O_2\pi_g$ hybrid orbitals are computed at much lower energies (Figure 2). In fact, IEH calculations in the Pauling geometry on $O_2MnP$ and $ImO_2FeP$ yield remarkably similar $d_\pi,O_2\pi_g$ hybrid orbital energies.[19] The oxyiron porphyrins (oxyhemes) exhibit normal-type absorption spectra with an additional feature at ~900 nm. This near-infrared band has been assigned[18] to porphine $\pi \rightarrow d_\pi,O_2\pi_g$ transitions on the basis of detailed analysis of their single crystal, MCD, and CD spectra and the calculations. Thus it is reasonable to expect normal optical spectra for oxymanganese porphyrins as well, should dioxygen bind in the Pauling mode.[25]

For optimal mixing of the charge-transfer and Soret transitions, the porphine $e_g(\pi^*)$ and the $d_{yz} + O_2\pi_{gz}$ orbitals should possess comparable energies. Nonetheless, for the Griffith models with the most favorable pyrrole N···O contacts (Table I) the $d_{yz} + O_2\pi_{gz}$ lies somewhat below the $e_g(\pi^*)$ (Figure 3). Actually, IEH calculations systematically underestimate charge-transfer transition energies,[18,26] possibly because the calculated orbital energies are directly affected by the atomic charge densities, and charge-transfer transitions result in considerable charge redistributions not reflected by ground-state calculations. Figure 6 illustrates the effect of $\pi \rightarrow \pi^*$ and charge-transfer excited-state configurations on the orbital energies of a staggered model with the Mn displaced 0.51 Å from the porphine plane, a $Mn-O_2$ midpoint distance of 1.85 Å and a peroxo dioxygen distance. The $\pi \rightarrow \pi^*$ promotion leaves the orbital energies virtually unchanged relative to the ground state since the excitation is localized on the porphine and there is no net charge redistribution between porphine, metal, and $O_2$. However, the porphine $\pi \rightarrow$ Mn $d,O_2\pi_g$ promotion raises the d and $O_2$ orbital energies significantly and leads to appreciable mixing between the porphine $e_{gy}(\pi^*)$ and the $d_{yz} + O_2\pi_{gz}$ orbitals (since they have the same symmetry). Hence, excited-state calculations corroborate our assignment of the hyperspectra.

Oxymanganese porphyrins also display a fairly intense red band at ~800 nm.[4] This band can be assigned to a $d_{z^2} \rightarrow e_g(\pi^*)$ transition which is dipole allowed and might gain intensity by borrowing from the porphine $a_{2u}(\pi) \rightarrow e_g(\pi^*)$ transitions. Indeed, the $d_{z^2}$ and $a_{2u}(\pi)$ orbitals always mix to some degree when the metal is out-of-plane (Figure 4). The calculations on pyridine and Griffith oxy complexes have $d_{z^2}$ and $a_{2u}(\pi)$ mixed to an equivalent extent (~20%), suggesting that the pyridine complexes ought to exhibit $d_{z^2} \rightarrow e_g(\pi^*)$ transitions as well. Since (py)-MnTPP absorbs only very weakly in the near-infrared, this transition apparently occurs at higher energy where it is masked by the porphine absorbance. Correcting the orbital energy differences of Figure 2 with suitable exchange terms[27] appropriately places the $d_{z^2} \rightarrow e_g(\pi^*)$ transition for the pyridine complex under the tail of the visible $\pi \rightarrow \pi^*$ bands, at 665 nm. A similar correction places the $d_{z^2} \rightarrow e_g(\pi^*)$ transition of the Griffith oxy complex at 795 nm vs. the ~800 nm observed experimentally.

**Staggered vs. Eclipsed Dioxygen Orientation.** The Griffith model which yields best agreement with the $^{17}O$ EPR results has

(25) Strictly speaking, one cannot deduce relative transition energies from IEH orbital energy differences alone when comparing metalloporphyrin systems with different total spin, because of the neglect of exchange terms.[18,21b] However, even when the larger exchange term for $O_2MnP$ is taken into account, the predicted $\pi \rightarrow d_\pi,O_2\pi_g$ transition energies for the Pauling mode are too low to account for the hyperspectra.

(26) Gouterman, M.; Hanson, L. K.; Khalil, G.-E.; Leenstra, W. R.; Buchler, J. W. *J. Chem. Phys.* **1975**, *62*, 2343–53.

(27) Exchange terms for the $d_{z^2} \rightarrow e_g(\pi^*)$ transitions were calculated in the manner of ref 18. For the $S = {}^5/_2$ pyridine complex, the exchange correction to the 0.63 eV orbital energy difference is 1.23 eV, giving a total transition energy of 1.86 eV (665 nm). For the $S = {}^3/_2$ Griffith oxy complex, the exchange correction to the 0.96 eV orbital energy difference is 0.60 eV, giving a total transition energy of 1.56 eV (795 nm). Note that the pyridine complex has twice the exchange correction of the oxy complex.

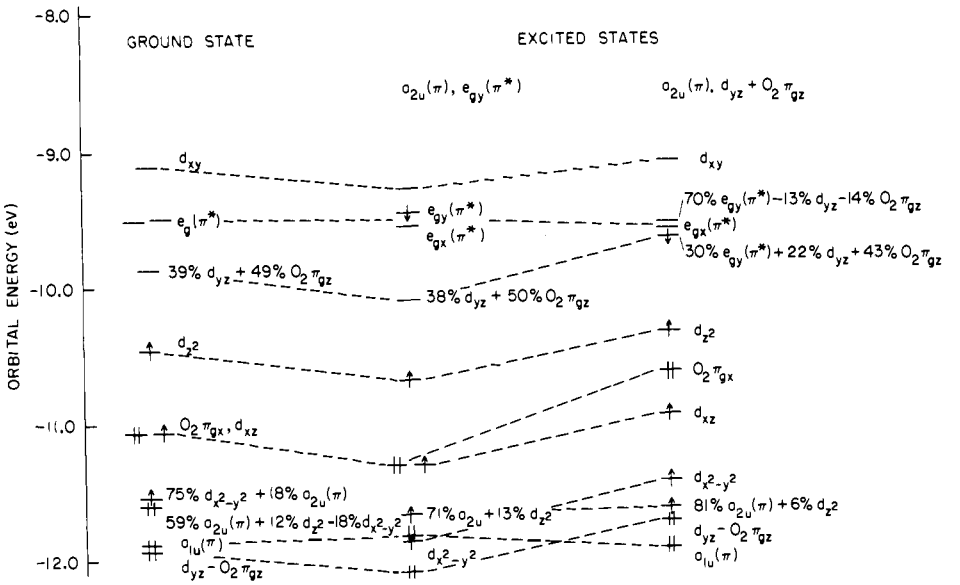


**Figure 6.** Orbital energies calculated for the ground state (left) and two excited states, porphine $a_{2u}(\pi) \rightarrow e_g(\pi^*)$ (center) and porphine $a_{2u}(\pi) \rightarrow d_{yz} + O_2\pi_{gz}$ (right), of an oxyMn porphine in the Griffith mode. Mn–Ct = 0.51 Å, O–O = 1.49 Å, Mn–$O_2$ midpoint = 1.85 Å, and O–O is staggered with regard to the pyrrole nitrogens.

the dioxygen staggered relative to the porphinato nitrogens. Two crystal structures of metalloporphyrins with edge-on-bound $O_2$, peroxotitanium(IV) octaethylporphine ($O_2$TiOEP)[28] and *trans*-diperoxomolybdenum(VI) tetra-*p*-tolylporphine,[29] show the dioxygen eclipsing the pyrrole nitrogens. The $O_2$TiOEP seemingly bears closest analogy to the oxymanganese porphyrins as the titanium is five-coordinate, 0.62 Å out-of-plane, and the O–O distance is 1.445 Å. An eclipsed structure for $O_2$TiOEP and a staggered structure for oxyMn complexes can be rationalized in terms of IEH calculations.

In a staggered conformation the metal $d_{xy}$ and $O_2\pi_{gx}$ orbitals are pure and unmixed, whereas in an eclipsed conformation the $d_{xy}$ and the $O_2\pi_{gx}$ mix to form a bonding and an antibonding hybrid orbital pair (Figure 4). It has been suggested[30] that for the eclipsed oxyTi complexes, only the bonding partner (predominantly $O_2\pi_{gx}$) is occupied, leading to a net stabilization. This explanation requires that the titanium $d_{xy}$ lie higher in energy than the $O_2\pi_{gx}$, and, indeed, IEH calculations on isoelectronic titanium and manganese porphine complexes[26] place the Ti d orbitals at much higher energies than the Mn d orbitals. In the oxymanganese case, the metal $d_{xy}$ (singly occupied) lies below the doubly occupied $O_2\pi_{gx}$. Thus eclipsing the dioxygen should result in a net *destabilization*, since the antibonding partner of the $d_{xy}$,$O_2\pi_{gx}$ orbital mixing is predominantly the $O_2\pi_{gx}$.

**Oxidation State Description.** The double occupancy of the dioxygen $\pi_{gx}$ orbital and the single occupancy of three orbitals having predominantly d character in the Griffith models support the $Mn^{IV}O_2^{2-}$ valency formalism.[2,4,5] However, a formal description of the oxidation state solely in terms of the $O_2$Mn core ignores the contribution of the porphyrin ring. In fact, the porphyrin ring compensates more for the charge density of an axial ligand than the manganese does. Table I lists the total charge densities for ligand, Mn, and porphine ring for calculations without an axial ligand and with electron-donating (pyridine) and electron-withdrawing (dioxygen) ligands. The net charge on the ring ranges from negative for the positive pyridine to positive for the negative dioxygen. The metal is most positive in the oxy complexes and probably can be characterized as "Mn(III)". Even so, the hyperspectra of the oxy complexes are not diagnostic of the charge on the manganese[31] but depend on the energy of a $d_{yz}$,$O_2\pi_{gz}$ hybrid orbital. The $O_2$ can best be described as a peroxo ($O_2^{2-}$) moiety to which charge transfer has taken place from both the metal and the ring.

**Concluding Remarks.** The dioxygen ligand with its low-lying $\pi_g$ orbitals interacts with the manganese d orbitals to profoundly modify the electronic structure of manganese porphyrins, as evidenced by their optical and EPR spectra. We have shown all the experimental data to be fully compatible with IEH and ligand field calculations on models with a $d^5$ odd-electron configuration and the dioxygen bound in the Griffith mode, but *not* in the Pauling mode.[32] This result would be amenable to verification by infrared and resonance Raman spectroscopy which should differentiate between peroxo and superoxo dioxygen[33] and symmetric vs. asymmetric binding.

The question arises as to why the ab initio calculations[14] favored the Pauling model. This prediction was based upon computations on eclipsed models with a small Mn out-of-plane displacement and short Mn–O distances, which lead to extremely short oxygen to pyrrole nitrogen distances for the Griffith geometry: O···N ≈ 2.3 Å (Table I), which is 0.6 Å shorter than the sum of the van der Waals radii of the two atoms. Because the ab initio method converges by minimizing the total energy of the molecule, a Griffith model with such tight O···N contacts should be unstable relative to a Pauling model. With these same coordinates, the

(28) Guilard, R.; Latour, J.-M.; Lecomte, C.; Marchon, J.-C.; Protas, J.; Ripoll, D. *Inorg. Chem.* **1978**, *17*, 1228–37.
(29) Chevrier, B.; Diebold, T.; Weiss, R. *Inorg. Chim. Acta* **1976**, *19*, L57–8.
(30) Ellinger, Y.; Latour, J. M.; Marchon, J. C.; Subra, R. *Inorg. Chem.* **1978**, *17*, 2024–6.

(31) Hyperspectra in Mn(III) porphyrin complexes with negligible d, axial ligand orbital mixing have been postulated to arise from porphine $a_{1u}$, $a_{2u}(\pi) \rightarrow d_\pi$ ($d_{xz}$, $d_{yz}$) charge-transfer transitions.[10,26]
(32) A recent communication (Lever, A. B. P.; Wilshire, J. P.; Quan, S. K. *J. Am. Chem. Soc.* **1979**, *101*, 3668–9) suggests on the basis of visible and IR absorption spectra, that, in contrast to $O_2$Mn porphyrins, dioxygen binds to manganese phthalocyanine (Pc) in the end-on, Pauling geometry. If this interpretation proves to be correct, then why the dioxygen binds differently to MnP and MnPc may be rationalized in terms of steric constraints between the $O_2$ and the pyrrole nitrogens. MnP without axial ligands has a nonplanar metal (the Mn is displaced 0.19 Å from the porphine ring[3]) and complexation of a fifth ligand is known to induce even greater Mn nonplanarity (ref 3 and 22 and Scheidt, W. R.; Hatano, K.; Rupprecht, G. A.; Piciulo, P. L. *Inorg. Chem.* **1979**, *18*, 292–9). As seen in Table I, reasonable Griffith geometries are possible when the metal is nonplanar. However, the Mn of MnPc is coplanar with the macrocycle (Kirner, J. F.; Dow, D.; Scheidt, W. R. *Inorg. Chem.* **1978**, *15*, 1685–90. Mason, R.; Williams, G. A.; Fielding, P. E. *J. Chem. Soc., Dalton Trans.* **1979**, 676–83). If the Mn of MnPc remains essentially coplanar upon complexation of dioxygen, the Pauling geometry is the only energetically feasible way the $O_2$ can bind.
(33) Preliminary IR results do tend to corroborate the Griffith model. Jones, R. D.; Budge, J. R.; Ellis, Jr., P. E.; Linard, J. E.; Summerville, D. A.; Basolo, F. *J. Organomet. Chem.* **1979**, *181*, 151–8.

IEH method, which includes no repulsive terms, still supports Griffith binding of dioxygen. Indeed, a very recent publication by Dedieu et al.[14b] notes that even the ab initio calculations are not inconsistent with the Griffith model in a staggered mode when the Mn is displaced a large distance from the porphine plane.

The present calculations suggest the following as the most probable Griffith geometry for oxymanganese porphyrins: (1) The manganese is most likely ~0.5 Å rather than ~0.2 Å out-of-plane because tighter metal–dioxygen bonding is possible with greater Mn displacement from the ring. (2) The dioxygen has a long bond, close to the peroxo distance of 1.49 Å, which improves its electron-acceptor capability. The above parameters give molecular orbital energies most consistent with the optical spectra and are consonant with the distances found in the crystal structure of $O_2Ti^{IV}OEP$. (3) The dioxygen is staggered with regard to the porphinato nitrogens on the basis of the net destabilization predicted by the MO's for an eclipsed structure and best agreement with $^{17}O$ hyperfine splittings.

**Acknowledgments.** L.K.H. wishes to thank Jack Fajer and Ronald H. Felton for valuable discussions. This work was supported by the Division of Chemical Sciences, U.S. Department of Energy, under Contract No. EY76-C-02-0016 at BNL and by the National Science Foundation (Grant PCM76-81304) and the National Institutes of Health (Grant HL-13531) at Northwestern University.

## Appendix: Spin Hamiltonian Parameters

The EPR studies[2,4,5] support an $S = {}^3/_2$ spin state for $O_2MnP$. In addition, the species exhibit two resolved hyperfine couplings for $^{55}Mn$, $(A^{Mn}, C^{Mn}) \approx (53, 83) \times 10^{-4}$ cm$^{-1}$. $^{17}O$ enrichment yields no resolved $^{17}O$ hfs but causes a line broadening which was analyzed by computer simulations to reflect $^{17}O$ hf values of $(A^O, C^O) \approx (2.8, 2.3) \times 10^{-4}$ cm$^{-1}$. The signs of the hfs and the orientations of the $(A^{Mn}, A^O)$ and $(C^{Mn}, C^O)$ axes with respect to the $O_2MnP$ symmetry directions are not known.

The IEH wave functions make it possible to calculate the $^{55}Mn$ and $^{17}O$ hyperfine values by assuming a particular configuration with three unpaired electrons. In the staggered Griffith geometry, the orbitals involved may be written (Figures 2 and 4) as eq 1.

$$x^2 - y^2 = a\mathrm{d}_{x^2-y^2} + \ldots \quad (1)$$

$$z^2 = b\mathrm{d}_{z^2} + \beta \mathrm{O}_2\pi_{uz} + \ldots$$

$$xz = c\mathrm{d}_{xz} - \gamma \mathrm{O}_2\pi_{ux} + \ldots$$

$$\pi_{gx} = \mathrm{O}_2\pi_{ux}$$

The diagonal elements of the anisotropic $^{55}Mn$ hyperfine splittings (hfs) interaction take the form of eq 2

$$\mathbf{T}^{Mn} = [T_x, T_y, T_z] = \frac{2P^{Mn}}{21}[\hat{a}^2 - \hat{b}^2 - 2\hat{c}^2, \hat{a}^2 - \hat{b}^2 + \hat{c}^2, -2\hat{a}^2 + 2\hat{b}^2 + \hat{c}^2] \quad (2)$$

where $\hat{t}^2 = t^2\epsilon$ and $\epsilon = 1$ or 0 when a d orbital is either half-filled or empty and $t^2$ is the Mulliken population of that d orbital, given as a percentage in Figures 2, 4, and 6. The electron–nuclear coupling parameter $P^{Mn} = g_e g_{Mn} \beta_e \beta_n \langle r^{-3} \rangle_{3d}$ should be comparable to the free-ion values, $P_0^{Mn}(4+) = 235 \times 10^{-4}$ cm$^{-1}$ for $Mn^{4+}$ and $P_0^{Mn}(3+) = 210 \times 10^{-4}$ cm$^{-1}$ for $Mn^{3+}$.[34] Similarly, the diagonal elements of the anisotropic $^{17}O$ hfs interaction take the form of eq 3

$$\mathbf{T}^O = \frac{-T_0}{6}\left[-\frac{+\hat{\beta}^2 + \hat{\gamma}^2 + \epsilon(\pi_{gx})}{2}, -\frac{\hat{\beta}^2}{2} + \hat{\gamma}^2, \hat{\beta}^2 - \frac{\hat{\gamma}^2}{2}\right] \quad (3)$$

where $T_0 = 4g_e g_N \beta_e \beta_n \langle r^{-3} \rangle_{2p}/5 = 93 \times 10^{-4}$ cm$^{-1}$.[35] The isotropic $^{17}O$ hfs is

$$a^O = -\frac{1}{6}(\hat{\beta}^2 + \hat{\gamma}^2 + \epsilon(\pi_{gx}))Q_\infty{}^O \quad (4)$$

where the $\sigma$–$\pi$ coupling parameter on the oxygen, $Q_\infty{}^O$, is $(37 \pm 5) \times 10^{-4}$ cm$^{-1}$.[36] Thus the observed $^{17}O$ hfs tensor can be expressed as eq 5. The **A** tensor for $^{55}Mn$ will similarly be the

$$\mathbf{A}^O = [A_x{}^O, A_y{}^O, A_z{}^O] = [T_x{}^O + a^O, T_y{}^O + a^O, T_z{}^O + a^O] \quad (5)$$

sum of $\mathbf{T}^{Mn}$ and an isotropic hfs, but, there is no simple relationship analogous to eq 4 for estimating $a^{Mn}$ from theory.

Possible odd-electron configurations and $Mn–O_2$ geometries for the $O_2MnP$ were tested by comparing the experimental $^{55}Mn$ and $^{17}O$ hfs with values obtained by substituting the Mulliken populations from the IEH calculations (Figures 2, 4, and 6) into eq 2–4. For a given configuration to be viable, $P^{Mn}$ (eq 2) must be close to the values spanned by $P_0{}^{Mn}$ (3+) and $P_0{}^{Mn}$ (4+), and the $^{17}O$ hfs computed from eq 3 and 4 must be consistent with the small experimental $^{17}O$ couplings.

**Griffith Geometry. $O_2$ Staggered.** (a) Placing one electron in the top three occupied MO's produces the odd-electron configuration of $(z^2)^1(xz)^1(\pi_{gx})^1$ which corresponds to two unpaired electrons in d orbitals and one on dioxygen. The only assignments of $^{55}Mn$ hyperfine couplings to porphyrin axis directions which give values of $P^{Mn}$ at all close to the $P_0{}^{Mn}$ are $(A_y{}^{Mn}, A_z{}^{Mn}) = (+53, +83) \times 10^{-4}$ cm$^{-1}$ or $(-83, -53) \times 10^{-4}$ cm$^{-1}$. Both assignments give $P^{Mn} = 187 \times 10^{-4}$ cm$^{-1}$, ~20% less than $P_0{}^{Mn}$ (4+) and ~10% less than $P_0{}^{Mn}$(3+). This value is not sufficiently low to reject the configuration. However, the calculated $^{17}O$ hfs tensor is $\mathbf{A}^O = [-1.6, 24, -6.4] \times 10^{-4}$ cm$^{-1}$. The $y$ axis component, $A_y{}^O = 24 \times 10^{-4}$ cm$^{-1}$, is a factor of 10 larger than the experimentally deduced $^{17}O$ hfs of $2.5 \times 10^{-4}$ cm$^{-1}$. Thus the $^{17}O$ results clearly rule out a $d^2\pi^*$ configuration for the Griffith geometry.

(b) The lowest energy configuration which occupies three metal d orbitals is $(x^2 - y^2)^1(xz)^1(z^2)^1$ (Figure 2) and corresponds to configuration b in ref 5. If the observed $^{55}Mn$ hfs are assigned to molecular axes as either $(A_x, A_z) = (-53, -83) \times 10^{-4}$ cm$^{-1}$ or $(+83, +53) \times 10^{-4}$ cm$^{-1}$, then $P^{Mn} = 219 \times 10^{-4}$ cm$^{-1}$, roughly midway between $P_0{}^{Mn}$(3+) and $P_0{}^{Mn}$(4+). Moreover, the calculated $^{17}O$ hfs tensor for this configuration is $\mathbf{A}^O = [-0.37, 2.0, 2.9] \times 10^{-4}$ cm$^{-1}$, and therefore the values of $(A_x, A_z)$ are sufficiently small to be in full accordance with experiment. The staggered Griffith geometry with a $(x^2 - y^2)^1(xz)^1(z^2)^1$ odd-electron configuration provides excellent agreement with the observed $^{55}Mn$ and $^{17}O$ hfs.

**Griffith Geometry. $O_2$ Eclipsed**: In the $d^3$ configuration analogous to (b), above, the $x^2 - y^2$ orbital is replaced by $xy = [a\mathrm{d}_{xy} + \alpha \mathrm{O}_2\pi_{gx} + \ldots]$. This has no effect on the $^{55}Mn$ hfs equations, but the admixture of $O_2$ in $xy$ causes an increase in the calculated $^{17}O$ hfs components, $\mathbf{A}^O = [2.5, 5.8, 5.6] \times 10^{-4}$ cm$^{-1}$, and predicts that one of the observed $^{17}O$ hfs is $5.6 \times 10^{-4}$ cm$^{-1}$, a value much larger than that obtained by computer simulations (Figure 5). Therefore the $^{17}O$ results favor a staggered over an eclipsed dioxygen orientation.

**Pauling Geometry.** (a) From Figure 2, the configurations with three odd electrons and the two lowest one-electron energies would place one electron each in $\mathrm{d}_{xz} - \mathrm{O}_2\pi_{gx}$, $\mathrm{d}_{yz} - \mathrm{O}_2\pi_{g\ddagger}$ and either $\mathrm{d}_{yz} + \mathrm{O}_2\pi_{g\ddagger}$ or $\mathrm{d}_{xz} + \mathrm{O}_2\pi_{gx}$. Either choice includes a pair of bonding, antibonding partners and is clearly unreasonable as a ground-state configuration for the complex. In addition, by equations similar to those presented above, we find, for example, by using $\mathrm{d}_{yz} \pm \mathrm{O}_2\pi_{g\ddagger}$, that the most favorable assignments of hfs axes gives $P^{Mn}$ either too large $(260 \times 10^{-4}$ cm$^{-1})$ or too small $(158 \times 10^{-4}$ cm$^{-1})$. The $^{17}O$ hf couplings along the $x$, $y$, and $z$ directions are computed to be (9.7, 1.6, 1.6) for the inner O and (11.4, 12.6, 12.6) for the outer O. Any choice of hfs axes would clearly lead to $^{17}O$ splittings

(34) Abragam, A.; Bleaney, B. "Electron Paramagnetic Resonance of Transition Ions"; Clarendon Press: Oxford, 1970.

(35) Morton, J. R.; Rowlands, J. R.; Whiffen, D. H. *Natl. Phys. Lab. (U.K.)*, Circulation No. BPR 1.3.

(36) (a) Cohen, A. H.; Hoffman, B. M. *J. Phys. Chem.* **1974**, *78*, 1313–21. (b) Symons, M. C. R.; Petersen, R. L. *Proc. R. Soc. London, Ser. B* **1978**, *201*, 285–300.

greater than $10 \times 10^{-4}$ cm$^{-1}$, far larger than experiment. Thus we reject these configurations.

(b) The next configuration in energy is illustrated in Figure 2, $(d_{x^2-y^2})^1(d_{xz} - O_2\pi_{gx})^1(d_{yz} - O_2\pi_{g*})^1$. Although this configuration corresponds to considerable unpaired spin density in the dioxygen $\pi^*$ orbitals, it is straightforward to generate the appropriate analogy to eq 2–4. Assigning the $^{55}$Mn hfs to the $y,z$ molecular axes gives $P^{Mn} = 205 \times 10^{-4}$ cm$^{-1}$ and to the $x,z$ molecular axes gives $P^{Mn} = 192 \times 10^{-4}$ cm$^{-1}$. The former value is essentially $P_0^{Mn}(3+)$, while the latter is only slightly lower. Thus, the $^{55}$Mn hfs calculated from the IEH wave functions are in agreement with experiment. The $^{17}$O hfs tensors are calculated to have axial symmetry, $A^O = -[10, -1, -1] \times 10^{-4}$ cm$^{-1}$ and $-[12, 3, 3] \times 10^{-4}$ cm$^{-1}$ for the near and far O atoms, respectively. Assignment of the $^{17}$O hfs to the $x,z$ axes is clearly inconsistent with experiment, for this would require the observed splittings to be $\sim$12 and $\sim$10 $\times 10^{-4}$ cm$^{-1}$, instead of the $\sim 2.5 \times 10^{-4}$ cm$^{-1}$ found. However, a fortuitous correspondence of the $^{55}$Mn hfs to the $y,z$ molecular axes would give $^{17}$O hfs that agree with the small observed values, in spite of the unpaired spin density on the dioxygen.

# $^{18}$O-Isotope Effect in $^{13}$C Nuclear Magnetic Resonance Spectroscopy. 2. The Effect of Structure

**John M. Risley and Robert L. Van Etten***

*Contribution from the Department of Chemistry, Purdue University, West Lafayette, Indiana 47907.* *Received December 26, 1979*

**Abstract:** A series of $^{18}$O-labeled organic compounds was synthesized in order to study further two aspects of the $^{18}$O-induced shift of natural abundance $^{13}$C NMR signals as compared to the respective $^{16}$O compounds. First, the direct effect of the hybridization of the carbon atom was studied in ethers. The observed effect was a significant decrease in the $^{18}$O-induced upfield shift when the carbon-atom hybridization was changed from sp$^3$ to sp$^2$. Second, the significance of the functional group on the $^{18}$O-isotope effect was evaluated. The experimental data reveal that the functional group plays an important role in affecting the magnitude of the $^{18}$O-induced shift. Large shifts are observed upon $^{18}$O-substitution in aldehydes and ketones while alcohols and phenols exhibit smaller shifts. Carboxylic acids show the expected intermediate shifts. In addition, a small but experimentally significant substituent-group effect on the carbonyl group $^{18}$O-isotope shift was observed upon changes in alkyl, aryl, or hydrogen substitution. The isotope-induced shift is discussed from a semitheoretical standpoint on the basis of known experimental results and theoretical predictions. In accord with these expectations, the $^{18}$O shift on the $^{13}$C resonance position is dependent both upon the chemical nature and the number of oxygens covalently bonded to the carbon atom.

## Introduction

We recently reported the existence of an $^{18}$O-isotope effect on $^{13}$C NMR spectra.[1] Related examples of the effects of isotopic substitution on nuclear magnetic resonance signals have been known for a number of years. Ramsey and Purcell[2] predicted an isotope effect on nuclear magnetic resonance signals and Wimett[3] first observed the difference in the molecular shielding factors for $^2H_2$, $^2H^1H$, and $^1H_2$. However, it was not until the $^2$H-isotope effects on $^{19}$F NMR[4] and $^1$H NMR[5] were reported that additional studies were begun on the isotope effect. The primary areas of interest were the $^2$H-isotope and $^{13}$C-isotope effects on $^1$H and $^{19}$F NMR. Batiz-Hernandez and Bernheim[6] reviewed the isotope effect on nuclear magnetic resonance signals through 1966.

Since then isotopic shifts involving other nuclei have been described. The primary $^2$H-isotope effect on $^{19}$F NMR was observed in gaseous $^2$HF.[7] Supporting evidence for the $^{34}$S-isotope effect, as well as the $^{13}$C-isotope effect, in $^{19}$F NMR was obtained with fluorine-labeled thiophene.[8] Deuterium-isotope effects were observed in $^{11}$B NMR,[9] $^{13}$C NMR,[10-12] $^{14}$N NMR,[9] $^{15}$N NMR,[9,13] $^{17}$O NMR,[14] and $^{31}$P NMR.[15] An additional $^{13}$C-isotope effect[16] and a $^{34}$S-isotope effect[17] in $^{13}$C NMR were observed. $^{34}$S was shown also to exert an isotope effect on the $^{95}$Mo NMR signal.[18] $^{18}$O was observed to exert an isotope effect on the $^1$H NMR of [$^{18}$O]water which averaged $\sim$0.3 ppm upfield.[19] $^{18}$O also was observed to exert an isotope effect on $^{31}$P NMR,[20] $^{55}$Mn NMR,[21,22] and $^{95}$Mo NMR.[21]

The magnitudes of such isotope effects are found to be dependent on the chemical-shift range of the nucleus being observed, as well as upon the type of compound.[6] The experimental data also show that heavy-atom isotopic substitution generally causes an upfield shift in the resonance signal of the nucleus being observed. However, Kanazawa et al.[23] and Fraenkel et al.[24] reported

(1) Part 1: Risley, J. M.; Van Etten, R. L. *J. Am. Chem. Soc.* **1979**, *101*, 252–253.
(2) Ramsey, N. F.; Purcell, E. M. *Phys. Rev.* **1952**, *85*, 143–144.
(3) Wimett, T. F. *Phys. Rev.* **1953**, *91*, 476.
(4) Tiers, G. V. D. *J. Am. Chem. Soc.* **1957**, *79*, 5585.
(5) Tiers, G. V. D. *J. Chem. Phys.* **1958**, *29*, 963–964.
(6) Batiz-Hernandez, H.; Bernheim, R. A. *Prog. Nucl. Magn. Reson. Spectrosc.* **1967**, *3*, 63–85.
(7) Hindermann, D. K.; Cornwell, C. D. *J. Chem. Phys.* **1968**, *48*, 2017–2025.
(8) Rodmar, S.; Rodmar, B.; Sharma, M. K.; Gronowitz, S.; Christiansen, H.; Rosen, U. *Acta Chem. Scand.* **1968**, *22*, 907–920.
(9) Shporer, M.; Loewenstein, A. *Mol. Phys.* **1968**, *15*, 9–15.
(10) Maciel, G. E.; Ellis, P. D.; Hafer, D. C. *J. Phys. Chem.* **1967**, *71*, 2160–2164.
(11) Lebel, G. L.; Laposa, J. D.; Sayer, G. G.; Bell, R. A. *Anal. Chem.* **1971**, *43*, 1500–1501.
(12) Grishin, Y. K.; Sergeyev, N. M.; Ustynynk, Y. A. *Mol. Phys.* **1971**, *22*, 711–714.
(13) Litchman, W. M.; Alei, M., Jr.; Florin, A. E. *J. Chem. Phys.* **1969**, *50*, 1897–1898.
(14) Lutz, O.; Oehler, H. *Z. Naturforsch. A* **1977**, *32*, 131–133.
(15) Borisenko, A. A.; Sergeyev, N. M.; Ustynyuk, Y. A. *Mol. Phys.* **1971**, *22*, 715–719. Stec, W. J.; Goddard, N.; Van Wazer, J. R. *J. Phys. Chem.* **1971**, *75*, 3547–3549.
(16) Weigert, F. J.; Roberts, J. D. *J. Am. Chem. Soc.* **1972**, *94*, 6021–6025.
(17) Linde, S. A.; Jakobsen, H. J. *J. Magn. Reson.* **1975**, *17*, 411–412.
(18) Lutz, O.; Nolle, A.; Kroneck, P. *Z. Phys. A* **1977**, *282*, 157–158.
(19) Pinchas, S.; Meshulan, E. *J. Chem. Soc. D* **1970**, 1147–1148.
(20) Cohn, M.; Hu, A. *Proc. Natl. Acad. Sci. U.S.A.* **1978**, *75*, 200–203. Lutz, O.; Nolle, A.; Staschewski, D. *Z. Naturforsch. A* **1978**, *33*, 380–382.
(21) Buckler, K. U.; Hasse, A. R.; Lutz, O.; Müller, M.; Nolle, A. *Z. Naturforsch. A* **1977**, *32*, 126–130.
(22) Haase, A. R.; Lutz, O.; Müller, M.; Nolle, A. *Z. Naturforsch. A* **1976**, *31*, 1427–1428.
(23) Kanazawa, Y.; Baldeschwieler, J. D.; Craig, N. C. *J. Mol. Spectrosc.* **1965**, *16*, 325–348.
(24) Fraenkel, G.; Asahi, Y.; Batiz-Hernandez, H.; Bernheim, R. A. *J. Chem. Phys.* **1966**, *44*, 4647–4649.

0002-7863/80/1502-4609$01.00/0 